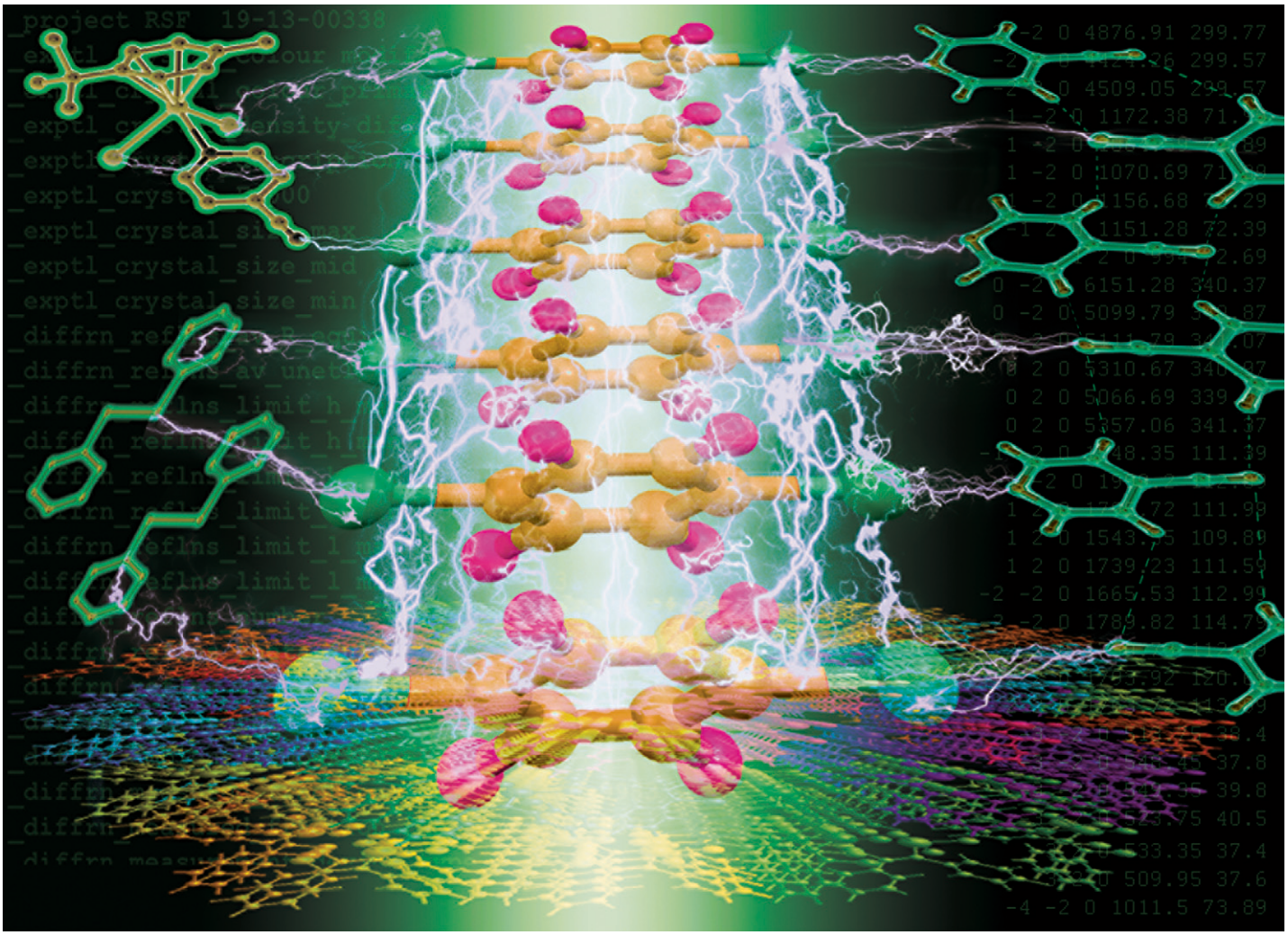

Showcasing research from Dr. Yury Torubaev's group at the Exchange Clusters Chemistry Lab, N.S. Kurnakov Institute of General and Inorganic Chemistry, Moscow, Russia.

The energy frameworks of aufbau synthon modules in 4-cyanopyridine co-crystals

Complementary combination of long-range synthon aufbau modules and energy frameworks allows the instrument to be used for visualization, interpretation and prediction of the supramolecular reactions. Energy ranking of aufbau synthon modules in the native crystals allows us to determine the modules that have a chance to be transferred to the co-crystal, possible pathways for their fragmentation, and further association with the synthon modules of the co-former.

As featured in:

See Y. V. Torubaev and I. V. Skabitsky, *CrystEngComm*, 2019, **21**, 7057.

ROYAL SOCIETY OF CHEMISTRY | Celebrating IYPT 2019

rsc.li/crystengcomm

Registered charity number: 207890

CrystEngComm

PAPER

Cite this: *CrystEngComm*, 2019, **21**, 7057

The energy frameworks of aufbau synthon modules in 4-cyanopyridine co-crystals†

Y. V. Torubaev * and I. V. Skabitsky

The supramolecular arrangement of 4-cyanopyridine (4CNpy) in its native crystal form and its co-crystals with halogen bond (XB) donors is discussed in terms of long-range synthon aufbau modules (LSAMs) and energy frameworks. Dissociations of 2D zigzag chains of parent 4CNpy into 1D dimers observed in its co-crystals are in good agreement with the aufbau model. Its co-formers, XB donors 1,4-$I_2(CF_2)_4$, C_2I_2, 1,3- and 1,4-$I_2C_6F_4$ (*m*- and *p*-DITFB), provide equal energy of I···N XBs, but perfluorinated iodo-alkane 1,4-$I_2(CF_2)_4$ and diiodoacetylene C_2I_2 cannot achieve the same strength of homomolecular aggregation as π–π stacking in columnar DITFB modules. As a result, DITFBs form I···N XBs with both N_{py} and N_{CN} nitrogen atoms of 4CNpy, while 1,4-$I_2(CF_2)_4$ and C_2I_2 only with the N_{py} atom. This is not a particular case of 4CNpy co-crystals, but in general, DITFB appears to be a more effective XB donor co-former than C_2I_2, 1,4-$I_2(CF_2)_n$ and other iodo-XB donors, which has similar potential to an iodine atom but lacks homomolecular aggregation. In supramolecular reactions of *p*-DITFB with (η^6-Ar)RuX_2(4CNpy) (Ar = *p*-cymene, X = Cl, I) bearing N_{py}-coordinated 4CNpy, the former gives definite preference to the XBs with the halogen atoms, but not to the CN group of the 4CNpy ligand.

Received 28th July 2019,
Accepted 25th September 2019

DOI: 10.1039/c9ce01174a

rsc.li/crystengcomm

Introduction

The cyanide ligand (CN^-) is extensively used in coordination chemistry as a bridging ligand for the synthesis of polymetallic cyanometallate complexes.[1] Studies of their intermolecular interactions during the past two decades have demonstrated that CN^- can be an effective acceptor of hydrogen bonds (HBs)[2] as well as halogen bonds (XBs).[3] In a practical sense, this leads to its use in crystal engineering and the design of functional materials. For example, the combination of CN ligands with electrophilic iodine atoms of functionalized TTFs allows fine-tuning of the electronic interactions in TTF-based hybrid molecular conducting materials.[4–6] The study of homoleptic cyanometallate complexes of Fe, Co and Cr (ref. 7) indicated that in the absence of competition with other XB-acceptors, the CN ligand in $[M(CN)_6]^{3-}$ is an effective π- or σ-XB acceptor for halogen atoms of bromo- and iodo-pyridinium counter ions. However, in water-solvated $(3,5\text{-}Br_2pyMe)_3[Cr(CN)_6]\cdot 4H_2O$, C–Br···O–H XBs are formed along with the C–Br···NC-M XBs. More examples of cyanometallate XB acceptors are summarized in a review by Brammer *et al.*[8]

Unlike chloride, which is a strong XB-acceptor if bonded to a transition metal atom, but quite a weak one when it is a substituent of an aliphatic or aromatic organic molecule,[8] an "organic" cyano-group (or nitrile) still shows weaker, but distinct propensity to accept XBs (*i.e.* from the electrophilic iodine atoms). Weaker C–H···NC-C HBs are also quite common – they were used in crystal engineering[9] and play a significant role in electrically conducting molecular materials.[10]

The most important examples of supramolecular architectures stabilized with I···NC-R XBs are the binary co-crystals of nitrile XB acceptors and iodo-XB donor organic molecules, where the I···NC XBs appear as a result of rational crystal design effort, so that we can describe them as the I···NC supramolecular synthon. In the Cambridge Structural Database (CSD[11]), there are 150 structures with short I···NC-R contacts and in 38 of them, the electrophilic iodine atom is a function of fluorinated (27 hits) or acetylene (11 hits) organic fragments. In certain cases, such I···NC systems cannot be obtained by traditional crystallization techniques, so co-sublimation was used for 1-adamantanecarbonitrile and *p*-DITFB to fabricate a co-crystal featuring an I···NC-C XB, resulting in a solid-state molecular rotor.[12] A representative collection of the illustrative examples of I···NC associated co-crystals (extracted from the CSD, see Table S1 ESI†) demonstrates that organic nitriles can form I···NC associates with traditional XB donors – perfluorinated aliphatic and

N.S. Kurnakov Institute of General and Inorganic Chemistry of Russian Academy of Sciences, Moscow, Russia. E-mail: torubaev@igic.ras.ru

† Electronic supplementary information (ESI) available. CCDC 1940710–1940714, 1941548 and 1955091. For ESI and crystallographic data in CIF or other electronic format see DOI: 10.1039/c9ce01174a

aromatic iodides. These I···NC short contacts can be major or additional stabilizing factors of the supramolecular self-assembly. A systematic structural study of XBs *vs.* HBs in competitive supramolecular systems[13] has demonstrated that the nitrile function of 4-cyano-pyridine (4CNpy) has a consistent preference for halogen bonding, while the pyridine moiety is engaged mostly in hydrogen bonding. The EWG-I···N_{py} synthon (EWG – electron withdrawing group) is extensively used in crystal engineering. In the CSD, there are 645 examples of I···N_{py} short contacts and 415 of them are with fluorinated iodo-organic and 57 with iodo-acetylenic XB donors.

In this work, we studied the co-crystallization of 4-cyanopyridine (4CNpy) with XB donor co-formers and described the structural results in terms of energy frameworks[14] and long-range synthon aufbau modules (LSAMs[15]). This combined approach, which allows energy-based representation of supramolecular reactions,[16] was used here to define LSAMs in the supramolecular reactions of 4CNpy with XB donor co-formers, and established the correlation between their energy frameworks and supramolecular reactivity, which can be used for the rational crystal design.

Results and discussion

Organic co-crystals of 4CNpy stabilized by I···N XBs

In the native 4CNpy crystal, the network of H···NC (2.489 Å) hydrogen bonds (HBs) binds its molecules into flat ribbons (see Fig. 1a). Assessment of the intermolecular interaction energy using Crystal Explorer 17.5/TONTO B3LYP-DGDZVP

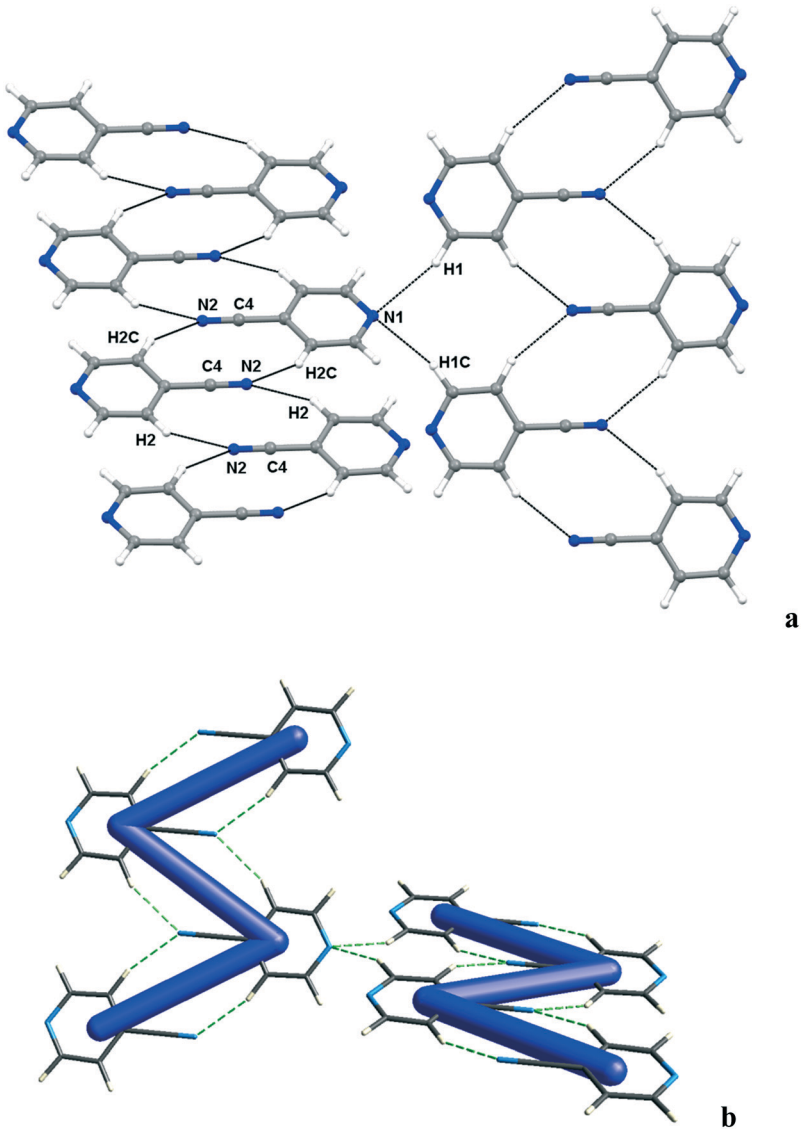

Fig. 1 Fragment of 4CNpy crystal packing, showing the H···NC stabilized flat ribbons (a) and respective zigzag energy frameworks (12 kJ mol^{-1} cut-off) (b). Selected intermolecular distances (Å): N(1)–H(1C) 2.589 and N(2)–H(2C) 2.489. The angle between the flat ribbon planes is 64°.

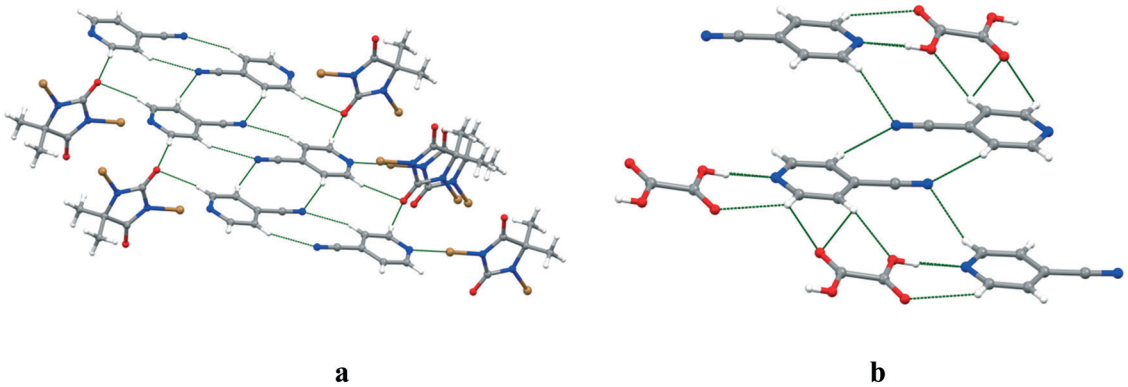

Fig. 2 Polymeric (a) and dimeric (b) H···NC HB associates of 4CNpy in its co-crystals with XB and HB donors 1,3-dibromo-5,5-dimethylimidazolidine-2,4-dione (EZIBIA) and oxalic acid (PAVGOK), respectively.

(CE 17.5) and its visualization as the energy framework[14] reproduce this visually observed packing pattern as a zigzag chain with the strongest (−25.5 kJ mol^{-1}) intermolecular interaction energy (see Fig. 1b and Fig. S1–S3 ESI†).

This illustrative energy framework of 4CNpy suggests that the 2D zigzag pattern, which is the strongest interaction of the parent crystal, has a chance to be transferred into its co-crystals as a whole or in parts, while the Npy···H HBs are the "weak links" and so, they the most probable candidates for the substitution by Npy···I XBs in the resulting co-crystals. On the other hand, the 2D (zigzag) LSAMs are less stable than, say 1D columnar modules,[15,17] so we can anticipate the fragmentation of the 2D flat ribbon into dimeric 1D associates. The statistic of the CSD[11] supports this suggestion: both polymeric (Fig. 2a[18]) and dimeric (Fig. 2b[19]) H···NC HB associates of 4CNpy can be found in its co-crystals with HB and XB donors, but the polymeric arrangement is rather rare as compared to the dimeric arrangement (see Table S2 ESI† for more examples).

We observed the latter dimeric pattern in the co-crystal of 4CNpy with the ditopic XB donor – 1,4-diiodooctafluorobutane (1,4-DIOFBu, see Fig. 3 and 4), obtained under slow solvent evaporation conditions. The chain-like aggregates in this 1,4-DIOFBu 4CNpy co-crystal (**1**) can be considered as 4CNpy dimers connected by a 1,4-DIOFBu linker, rather than trimer 4CNpy···1,4-DIOFBu···4CNpy fragments, associated with H···NC HBs.

We observed, similar to **1**, the I···N$_{py}$ XB stabilized trimeric associates 4CNpy···[ditopic XB linker]···4CNpy in the co-crystal of 4CNpy with another ditopic XB donor – 1,2-diiodoacetylene (C_2I_2 ·4CNpy (**2**), see Fig. 5a), obtained by the cooling of their heptane solution. In contrast to **1**, the HB stabilized dimeric associates of 4CNpy are absent in **2**. The CN nitrogen (N2) and β-hydrogen (H7) atoms are involved in hydrogen bonds and form a trimolecular junction, which does not allow the linear extension of the chain, but a 72.7° turn.

Utilization of *ortho*-, *meta*-, and *para*-isomers of diiodotetrafluorobenzene (DITFB) as the XB-donor co-formers for 4CNpy under the slow evaporation conditions resulted in the 1 : 1 co-crystals only for *p*- and *m*-DITFB and a colorless oily material for *o*-DITFB. The XRD investigation of *p*-DITFB – 4CNpy (**3**) and *m*-DITFB – 4CNpy (**4**) demonstrated that DITFB bonds with both pyridine and nitrile nitrogens of 4CNpy through the intermolecular I···N XB interactions (see Fig. 6a and 7a). The linear 1D chains in **3** cannot approach each other to form the C–CN···H–C hydrogen bonded dimers similar to those in the native 4CNpy or **1**, while in **4**, the directionality of the XB of the iodo substituents in *m*-DITFB directs the self-assembly of the zigzag chains of alternating 4CNpy and DITFB molecules. This zigzag pattern affords the formation of C–CN···H–C hydrogen bonded 4CNpy dimeric associates, which (along with H···F interactions) binds zigzag chains into the layers (see Fig. 7). These C–CN···H–C HBs are

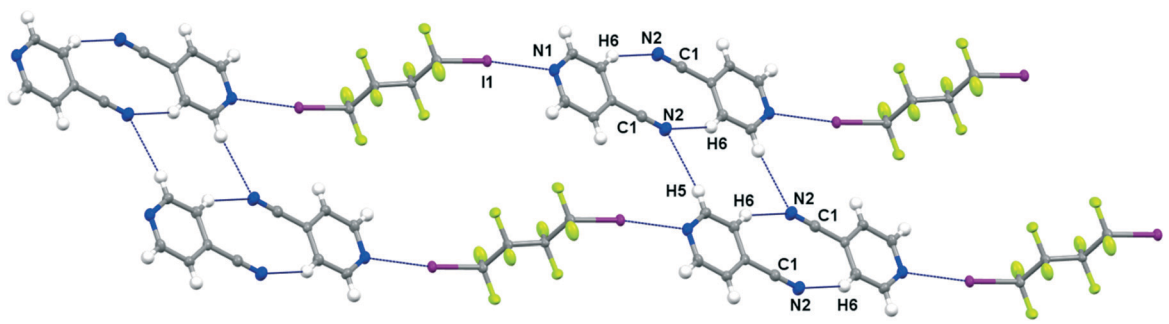

Fig. 3 The solid state structure of **1**. Selected intermolecular distances (Å): I(1)–N(1) 2.906(4), N(2)–H(6) 2.609(5), and C(1)–N(2) 3.481(6). Selected angles: C(7)–I(1)–N(1) 173.1(1). Dotted lines indicate XBs of the atoms with distances shorter than the sum of vdW radii.

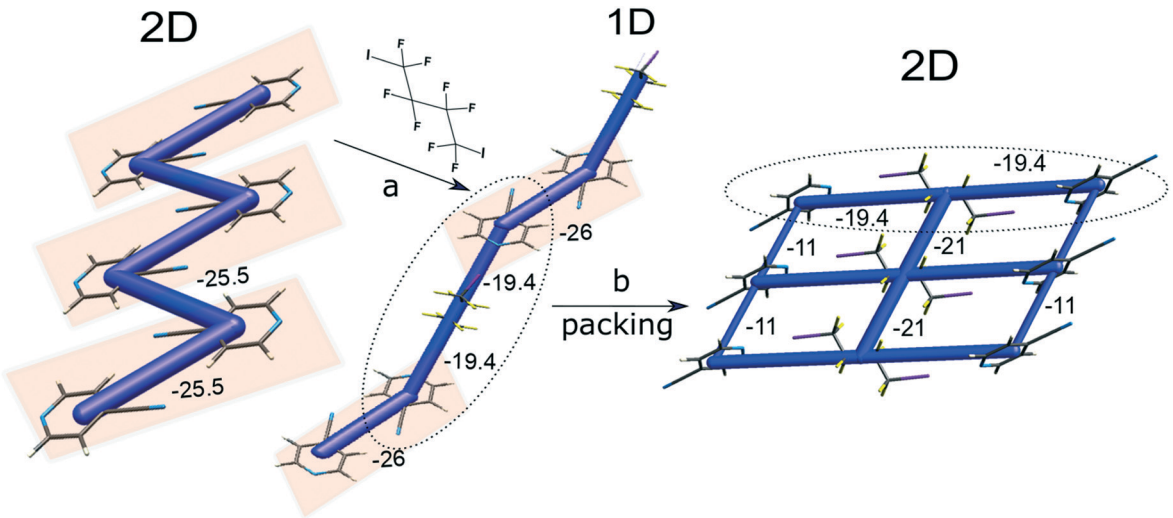

Fig. 4 Fragmentation of the 2D zigzag pattern in the native 4CNpy crystal into a dimeric fragment associated ditopic XB donor – 1,4-DIOFBu (a), and further packing of the resulting chains into 2D layers, stabilized by 4CNpy stacking and 1,4-DIOFBu I···F intermolecular interactions (b). The intermolecular interaction energy is given in kJ mol^{-1}. Notice similar (≃26 kJ mol^{-1}) energy values for dimeric 4CNpy fragments in the starting 4CNpy and its co-crystal **1**, which exceeds the energy of the I···Npy XB associated with 1,4-DIOFBu (–19.4 kJ mol^{-1}).

a part of the bifurcated system of XB/HB bonds I(2)···N(2)···H(3) (see Fig. 7a) and are significantly elongated (3.0 Å) as compared to 2.6 Å in **1** and accordingly, the intermolecular interaction energy in 4CNpy dimeric associates is lower in **4** (−20 kJ mol^{-1}) as compared to −26 kJ mol^{-1} in **2** (see Table S4 ESI†).

Our assessment of the intermolecular interaction energy in **1–4** (using Crystal Explorer 17.5 TONTO B3LYP-DGDZVP) demonstrated close energy values for the I···N_{Py} XBs (−19.4 kJ mol^{-1} (**1**), −22.4 kJ mol^{-1} (**2**) and −19.6 kJ mol^{-1} (**3**, **4**), see Table S4 ESI†). This is in good agreement with the equivalent maximum values (V_{max}) of the molecular electrostatic potential (MEP) on iodine atoms found for C_2I_2 (−195 kJ mol^{-1}) and reported earlier for 1,4-DIOFBu (−168 kJ mol^{-1} (ref. 20)) and 1,4-DITFB (−168.9 (ref. 21)).The intermolecular bonding which includes the I···N_{Py} XB is among the strongest in **1–4**, while I···N_{CN} XBs are absent in **1** and **2** and are rather weaker in **3** (−12.3 kJ mol^{-1}) and **4** (−11.6 kJ mol^{-1}). However, these I···N_{py} XBs (19.6 kJ mol^{-1}) in **3** and **4** are only second after the π–π stacking between *p*-DITFB molecules (−32 kJ mol^{-1} and −29 kJ mol^{-1} in **3** and **4** accordingly see Table S4 ESI†), which appears to be the strongest intermolecular interaction in **3** and **4**. The stacking of DITFB also tends to be the structure stabilizing factor in **3** and **4**.

In co-crystal **2**, the molecules of C_2I_2 forms weak homomolecular chains (−10.7 kJ mol^{-1}), which are in turn rather feebly associated with each other (−4 kJ mol^{-1}, see Fig. 5c). The low affinity of C_2I_2 for self-association makes side-by-side hydrogen bonding with 4CNpy more effective (−11.9 kJ mol^{-1}, see Fig. 5c, Table S4 ESI†) and therefore does not favor the packing pattern similar to **1**. In general, as it can be concluded from the analysis of the structures deposited in the CSD, the C_2I_2 ditopic "stick" has a definite structure-directing character,[22,23] but not a structure-forming one.

It worth noting here that the stabilizing and structure determining factor of π–π stacking in the columnar modules of halogenated aryl XB[24] and HB[25] donor co-formers was utilized for the solid-state template photochemical [2 + 2] cycloaddition in their co-crystals with trans-1,2-bis(4-pyridyl)ethylene (see Scheme S1 ESI†).

Analysis of the dispersion and electrostatic contribution to the full intermolecular interaction energy (using CE 17.5 Tonto B3LYP/DGDZVP) in **1–4** demonstrate that both I···N_{Py} and I···N_{CN}XBs are mostly electrostatically driven, while dispersion provides the major contribution to the association of 1,4-DIOFBu and stacking of *p*-DITFB (−32.7 kJ mol^{-1}) and 4CNpy (−10.9 kJ mol^{-1}, see Table S4 ESI†).

Hybrid organometallic XB co-crystals of 4CNpy

Halogen bonding is indeed a bridge between organic and coordination chemistry. It does not only brings together organic molecules and metal complexes into their respective hybrid materials, but also allows the use of more universal structural approaches and models. In the metal complexes 4CNpy (similarly to **1–4**), can be either a monodentate (Scheme 1a) or bridging ligand between two metal centers using both pyridine and nitrile nitrogens for coordination with two metal centers (see Scheme 1b).[26]

Furthermore, in the solid state, the molecules of $CymRuCl_2$(4CNpy) are associated with H···NC HBs between 4CNpy ligands, similar to **1** (see Fig. S4a ESI†). The packing

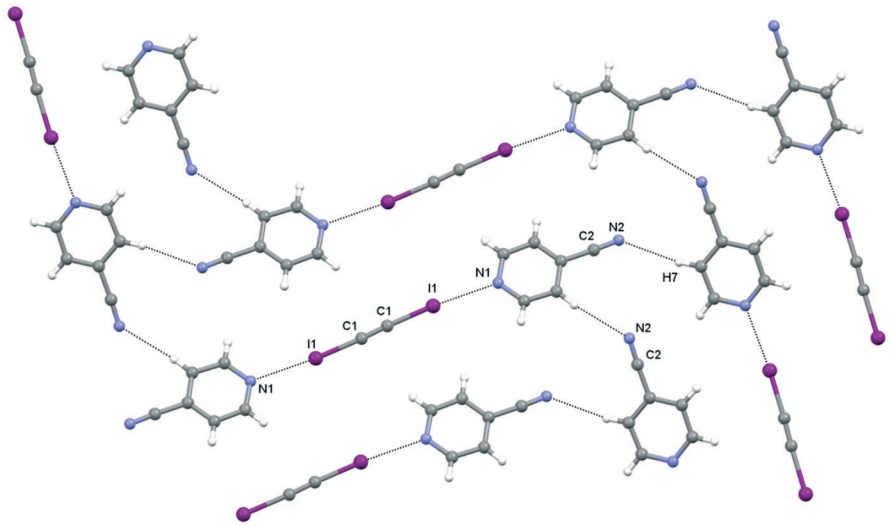

a

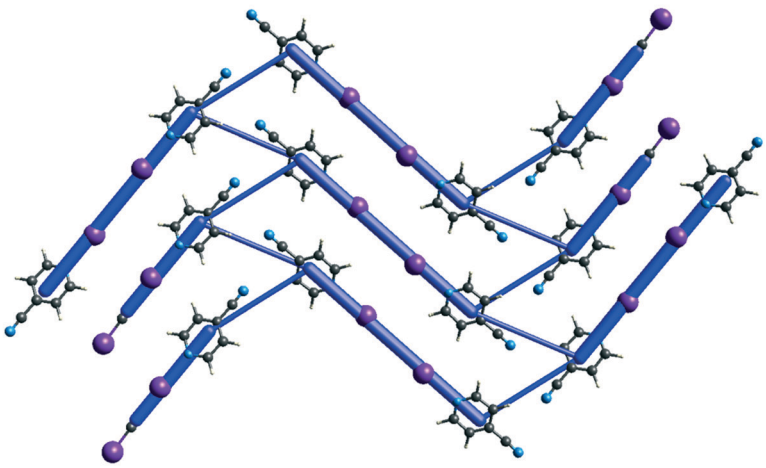

b

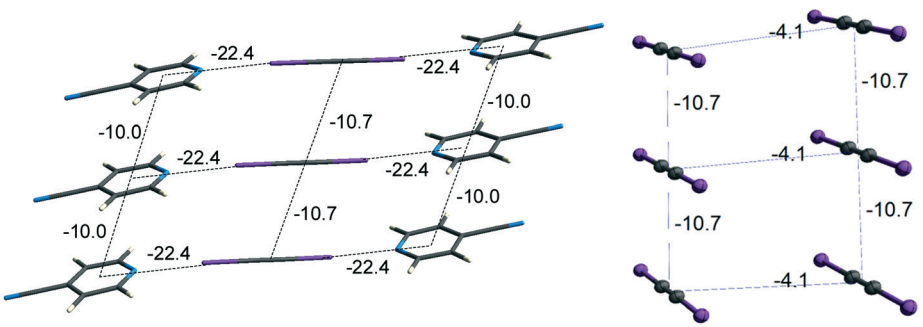

c

Fig. 5 (a) Fragment of the 1D chain in the solid state structure of **2**, showing the I···N_{Py} halogen bonded 1D trimer assemblies. Selected intermolecular distances (Å): I(1)–N(1) 2.819(5) and H(7)–N(2) 2.641. Selected angles (°): C(1)–I(1)···N(1) 175.9(2) and C(2)–N(2)···H(7) 138.8. Dotted lines indicate XBs of the atoms with distances shorter than the sum of vdW radii. (b) The zigzag energy framework of the layers (cut-off of 9 kJ mol^{-1}). (c) Energy of intermolecular interactions in the stacks of C_2I_2 and 4CNpy in **2**. Dotted lines link the centers of the molecules.

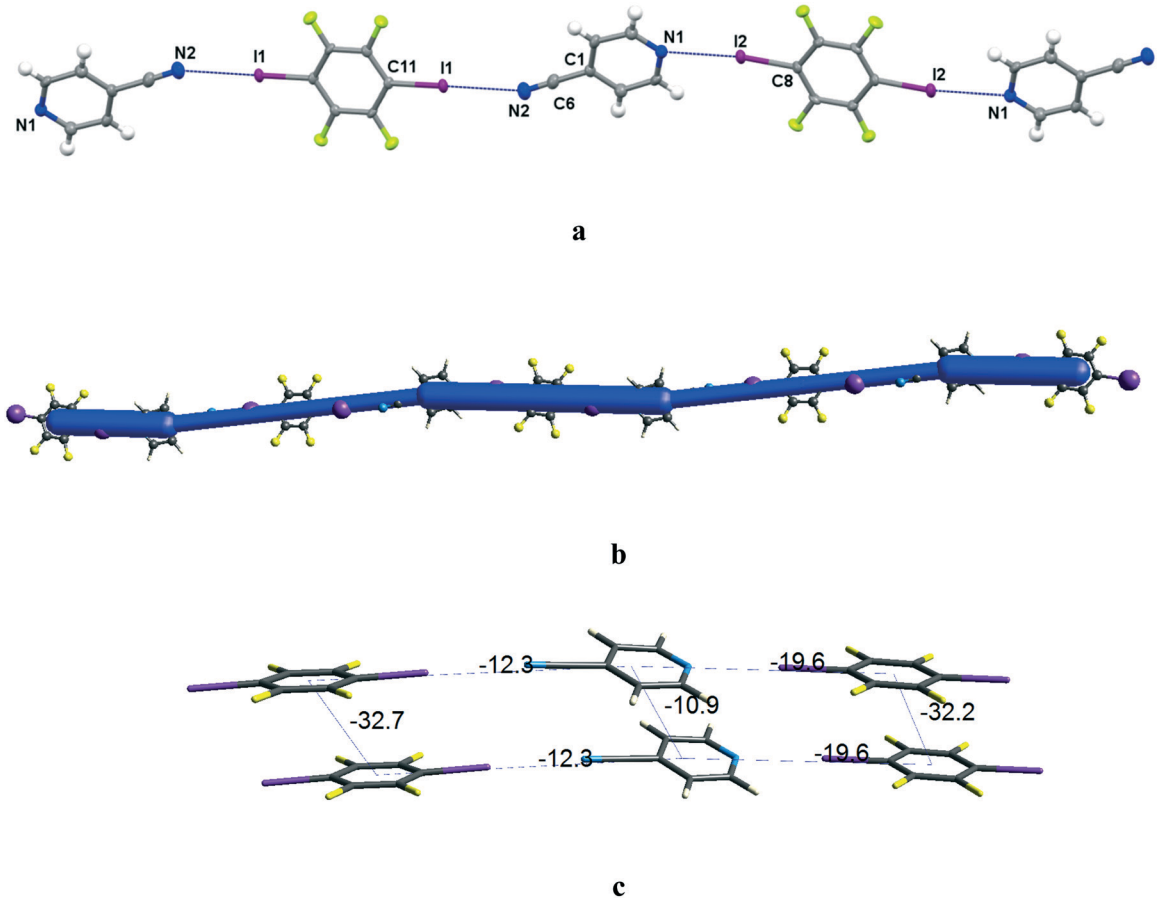

Fig. 6 (a) Fragment of the solid state structure of **3**, showing the fragment of I···N_{Py}/I···N_{CN} halogen bonded 1D-chain assemblies and (b) its energy framework (cut-off of 10 kJ mol^{-1}). Selected intermolecular distances (Å): I(1)–N(2) 3.08(1) and N(1)–I(2) 2.934(8). Selected angles: C(11)–I(1)–N(2) 179.4(3), C(6)–N(2)–I(1) 159.8(8), and C(8)–I(2)–N(1) 172.5(3). Dotted lines indicate XBs of the atoms with distances shorter than the sum of vdW radii. (c) Energy of intermolecular interactions in **2**. Dotted lines link the centers of the molecules.

of its iodide congener $CymRuI_2$(4CNpy), however, does not reveal any specific association (see Fig. S4b ESI†).

Besides the CN function of the 4CNpy ligand, the halide ligands are another possible XB accepting sites in $CymRuX_2$(4CNpy) (X = Cl, I). Evaluation of the XB acceptor strength based on the molecular electrostatic potential (MEP, see Fig. 8) does not allow confident prediction of the selectivity[27]‡ between Cl and CN functions in $CymRuCl_2$(4CNpy). The location of the V_{max} (−55.8 kcal mol^{-1}) area on the MEP surface of $CymRuCl_2$(4CNpy) is concealed between two Cl ligands, and therefore not accessible for XB interaction. The V_{max} of the nitrile function of the 4CNpy ligand (−34.6 kcal mol^{-1}) is equal or comparable to the MEP of most of the accessible area of Cl ligands (see Fig. 8 and Fig. S5 ESI†). From the same map (*ibid.*), we can notice the greater blue area on Cl as compared to CN, allowing more flexibility (Fig. 9).

It is noteworthy that V_{max} of the CN nitrogen in 4CNpy decreases from −37.4 kcal mol^{-1} in free 4CNpy§ to −34.6 kcal mol^{-1} in coordination with the $CymRuCl_2$ fragment (see Fig. S5–S6 ESI†). The natural result of electron withdrawing in the process of N_{py} donation to metal is in good agreement with the data on the increase of halogen bond donation in 4-iodopyridine upon the introduction of metal coordination on the N_{py} atom.[28]

Co-crystallization of *p*-DITFB with $CymRuX_2$(4CNpy) (X = Cl, I) from the slowly evaporating DCM solution afforded **1**:**1** (X = Cl, **5**) and **2**:**3** (X = I, **6**) binary crystals (see Scheme 2). In both co-crystals, *p*-DITFB forms halogen bonds (XBs) only with the halide ligands, but not with the nitrile function of 4CNpy (see Scheme 2).

A similar preference of C_6F_5I and *p*-DITFB for XBs with halide ligands instead of nitrile can be noted in their co-crystal with trimethylplatinum(IV) iodide complexes of CN

‡ ΔE cutoff value, as a boundary between two possible outcomes, should be between 20 and 40 kJ mol^{-1} (ref. 26).

§ Or −38 kcal mol^{-1} as calculated by Aakeröy *et al.*[13]

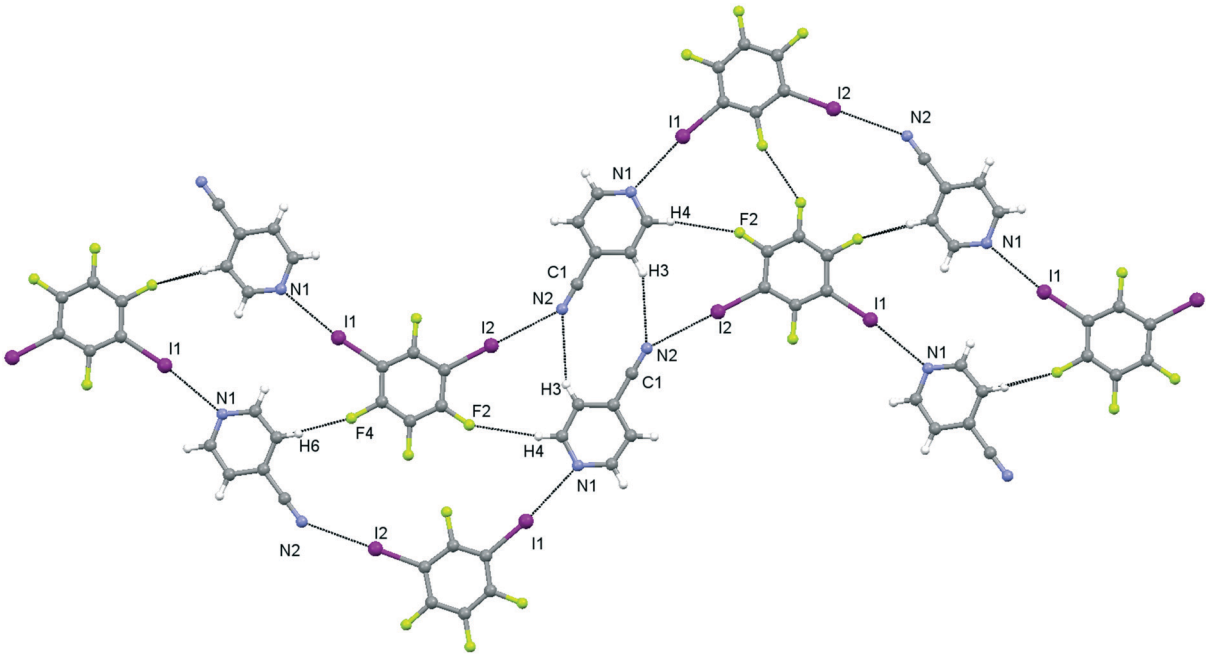

a

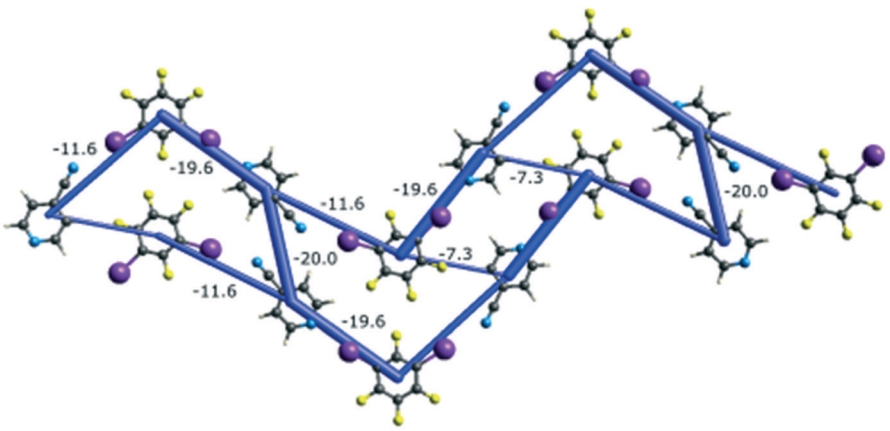

b

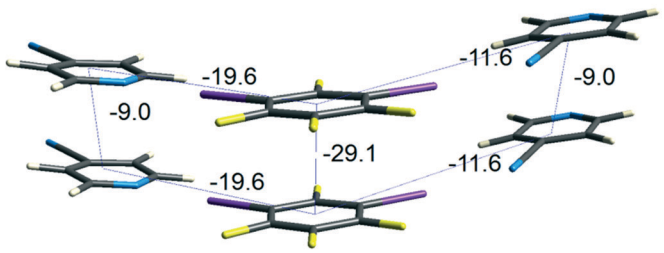

c

Fig. 7 (a) Fragment of the solid state structure of **4**, showing the fragment of I···N_{Py}/I···N_{CN} halogen bonded 2D zigzag chain assemblies. Notice the bifurcated HB/XB bond I(2)···N(2)···H(3). Selected intermolecular distances (Å): I(2)–N(2) 3.14(2), N(1)–I(1) 3.00(1), H(3)–N2 3.00, H(4)–F(2) 2.766, and F(4)–H(6) 2.393. (b) The energy framework (cut-off of 9 kJ mol^{-1}). (c) Energy of intermolecular interactions in **4**. Dotted lines link the centers of the molecules.

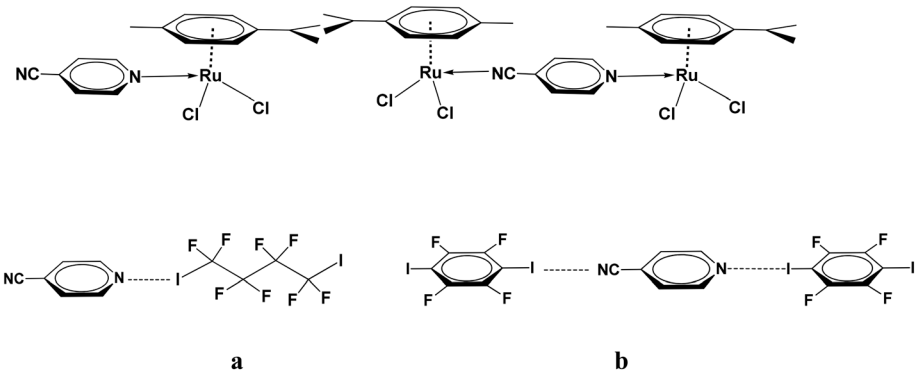

Scheme 1 (a) Mono- and (b) ditopic binding modes of 4CNpy in complex with cymene-ruthenium dichloride (intramolecular) and in the co-crystals with 1,4-DITFB (**3**) and 1,4-DIOFBu (**1**).

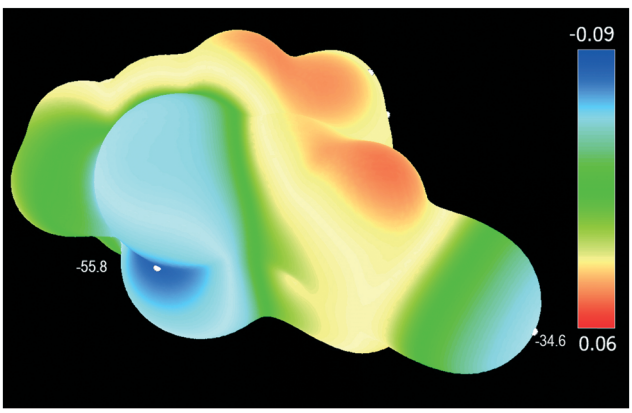

Fig. 8 Molecular electrostatic potential map of $CymRuCl_2(4CNpy)$ (0.002 e A^{-3} electron density isosurface). Notice the hardly accessible V_{max} (−55.8 kcal mol^{-1}) area on chloride ligands.

functionalized 2,2′,6′,2″-terpyridine (ref. 29, see Scheme S2 ESI†).

Two I···Cl XBs in **5** are of equal length (~3.17 Å), but have different geometries of Ru–Cl···I and C–I···Cl angles (see Fig. 3). Although, such geometries formally suggest assigning them as type I (I(1)–Cl(1)) and type II (I(2)–Cl(2)) XBs[30] (see Fig. 10), we should keep in mind the requirement of 90° angles which are quite flexible for metal chlorides and never achieved due to the strong and rather even (spherical) negative charge over the vdW surface of chloride (and directionality of its $3sp^3$ orbitals)[31] (see Scheme 3). In contrast to chloride, the iodide ligand has the unhybridized 5p orbitals, which are responsible for the 90° I···I–Ru angle in the case of genuine XBs (*ibid.*). The flexibility of the I···Cl–Co angle and difference in the directionality of the I···X–Ru halogen bond were noted recently in studies on $(bpy)_2CoCl_2$ (ref. 32) and $Ru(bpy)(CO)_2X_2$ (X = Cl, Br, I)[33] co-crystals with perfluorinated iodobenzenes.

In the crystals of **6**, each $CymRuI_2(4CNpy)$ molecule forms three different I···I XBs, providing the single $[CymRuI_2(4CNpy)_2(\mu\text{-DITFB})]$ and double-bridged $[CymRuI_2(4CNpy)_2(\mu\text{-DITFB})_2]$ chains (see Fig. 10). These I···I XBs has different geometries and energies, ranging from a quite strong type II to a rather weak type I (not to say mechanical) interaction. Although halogen bonding is just one of the parameters in the complex interplay of other intermolecular interactions and structural symmetry factors, which define the resulting supramolecular structure, **6** demonstrates once again that the angle (*e.g.* Ru–I···I) is a more important criterion than the distance for distinguishing the genuine halogen bond.

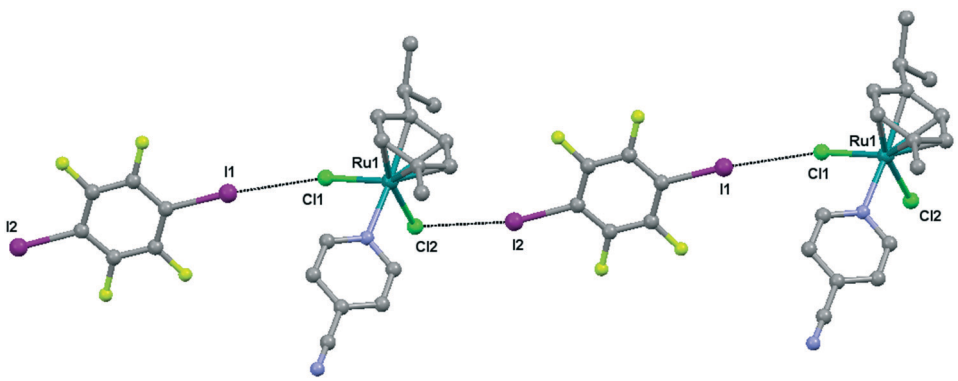

Fig. 9 Crystal structure diagram of **3**, showing the fragment of I···Cl halogen bonded polymeric chains $([CymRuCl_2(4CNpy)](\mu\text{-DITFB}))_n$. Hydrogen atoms are omitted for clarity. Selected intermolecular distances (Å): I(1)–Cl(1) 3.168(1) and I(2)–Cl(2) 3.169(1); angles: Ru(1)–150.81(5) and Ru(1)–Cl(2)–I(2) 109.56(5). Dotted lines indicate XBs of the Cl and I atoms with distances shorter than the sum of the Cl–I vdW radii.

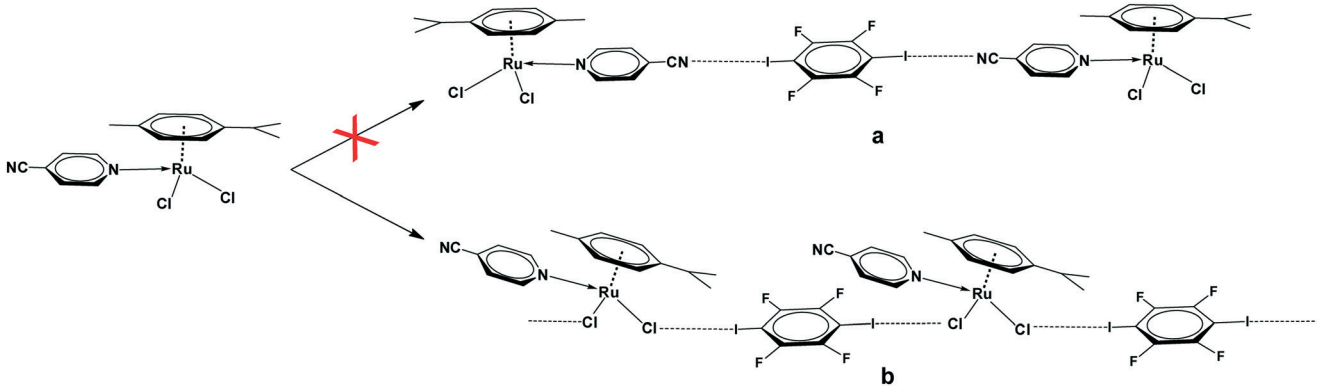

Scheme 2 Two possible arrangements of *p*-DITFB and $CymRuX_2(4CNpy)$: (a) I···CN XB associated trimer and (b) I···Cl XB associated polymeric chain (combinations of a and b are omitted for clarity).

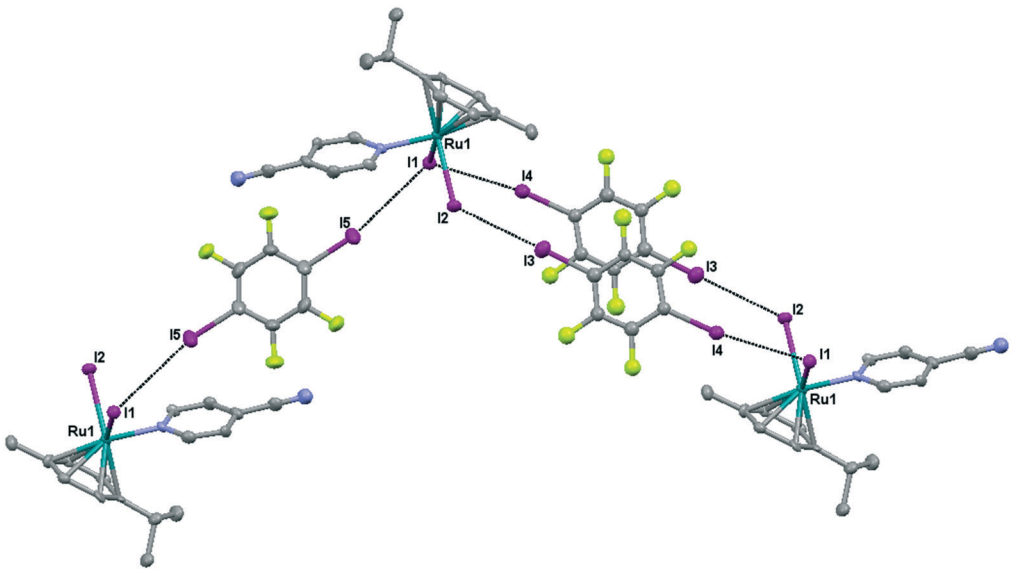

Fig. 10 Crystal structure diagram of **4**, showing the fragment of I···Cl halogen bonded polymeric chains $[(CymRuI_2(4CNpy))(\mu_2\text{-}DITFB)_2(CymRuI_2(4CNpy))(\mu\text{-}DITFB)]_n$. Hydrogen atoms are omitted for clarity. Selected distances (Å): Ru(1)–I(1) 2.7261(8), Ru(1)–I(2) 2.739(1), I(1)–I(5) 3.898(1), I(1)–I(4) 3.5666(9), and I(2)–I(3) 3.580(1). Selected intermolecular angles: Ru(1)–I(1)–I(5) 99.08(2), Ru(1)–I(1)–I(4) 97.80(2), and Ru(1)–I(2)–I(3) 126.60(3). Dotted lines indicate XBs of the I atoms with distances shorter than the sum of vdW radii.

Summary

In the organometallic co-crystals of $(\eta^6\text{-}p\text{-cymene})RuX_2(4CNpy)$ (X = Cl, I) with *p*-DITFB, the latter shows a definite preference towards the XB with halogen atoms over the CN group of the 4CNpy ligand.

In all the studied cases of the supramolecular reactions of 4CNpy with iodo-XB donors, the short-range N_{py} ···I-[EWG]-I···N_{py} synthon is realized. In the case of *m*- and *p*-DITFB XB donor co-formers, the R-CN ···I-[EWG]-I···NC-R supramolecular synthon is realized as well.

Supramolecular reactions of 4CNpy with HB or XB donors can proceed with the conservation of the H···CN HB stabilized flat ribbons, their fragmentation into the dimeric H···CN HB stabilized fragments, or dissociation of the latter in the resulting co-crystal. Fragmentation of the 2D zigzag modules of parent 4CNpy into 1D dimeric fragments in the co-crystals is in good agreement with the aufbau module model, which assumes the greater stability of 1D structures. In the case of XB donor co-formers like $1,4\text{-}I_2(CF_2)_4$, C_2I_2, and *m*- and *p*-DITFB, the depth of such fragmentation depends on the strength of the homomolecular association that they can provide and geometry factors. Strong π–π stacking in columnar DITFB LSAMs is a definite advantage as compared to the perfluorinated iodo-alkane $1,4\text{-}I_2(CF_2)_4$, which is equal to the DITFB energy of the I···N XB, but its F···I and F···F intermolecular interactions cannot provide the same strength of homomolecular aggregation. The energy of the I···N XB for C_2I_2 is slightly higher (−22.4 kJ mol^{-1}), but the energy of its homomolecular aggregates is twice less than that of $1,4\text{-}I_2(CF_2)_4$ (and thrice less than that of DITFB), so we cannot define reliable homomolecular synthon modules for C_2I_2. A stronger homomolecular LSAM provides greater contribution to the co-crystal lattice energy and this gives such LSAMs a

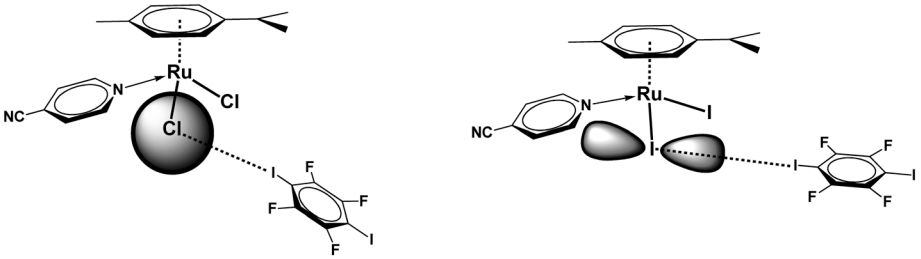

Scheme 3 Spherical chloride anion dictates the flexible directionality of the I···Cl–M halogen bond (a), while unhybridized 5p orbitals of more covalent iodine demand a 90° I···I–Ru angle for the respective I···I halogen bond.

certain advantage in comparison with the intermolecular interactions of the co-former LSAMs and as compared to the other XB donors. As a result, *m*- and *p*-DITFBs form I···N XBs with both nitrogen atoms of 4CNpy, while 1,4-$I_2(CF_2)_4$ and C_2I_2 – only with the pyridine nitrogen atom. In general, DITFBs appear to be more effective than 1,4-$I_2(CF_2)_n$ and C_2I_2 XB donor co-formers for various XB-acceptors. Certainly, these energetic considerations are in complex interplay with the geometric factors and a pair of **3** and **4** co-crystals is an illustrative example.

It is noteworthy that *p*-DITFB forms I··· π XB stabilized, tilted stacks only in one of its native polymorphs (putatively kinetic form ZZZAVM02 (ref. 34)), and aggregates in columnar modules in ~45% of its co-crystals (deposited in the CSD). The character of bonding in these *p*-DITFB stacks varies between π–π stacking and I··· π halogen bonding. A similar situation is noted for 1,4-DIOFBu, which is liquid at room temperature and its solid state structure is unknown, but in ~30% of its co-crystals, it aggregates into the I···F stabilized stacks.

The above energy frameworks of the synthon module approach for the co-crystal formation and observations of the effect of the LSAM strength on the co-crystal packing pattern are not limited to the compounds described here and create a wide perspective for further development of our understanding of the principles governing crystal formation.

Conclusion

Considering the energetic component in a complex interplay of the factors governing the packing patterns and crystallization, we can conclude that in halogen-bonded co-crystals, the packing pattern is defined by the energy of homomolecular synthon modules (LSAMs) and the energy of their interaction, rather than the intermolecular interaction in the pairs of donor and acceptor molecules. Ranking of homomolecular LSAMs in terms of their energy (in addition to statistic and intermolecular distances) allows definition of the LSAMs of native crystals which have a chance to be transferred into the co-crystals and the possible pathways for their fragmentation and further association with co-former LSAMs.

Although the energies of the LSAMs in the crystals of different substances cannot be directly compared, such ranking of LSAMs and corresponding energy frameworks can give us a hint on a "weak link" in a co-former, which is most likely to be affected, and the strongest one which is most likely to be transferred into the co-crystal intact. In our particular case, we can define the strongest I-[EWG]-I synthon module as that having the greater energy of homomolecular aggregation (provided that the energy of the I···N XB is the same or has close values, as in our case).

Therefore, complementary combination of long-range synthon aufbau modules (LSAMs[15]) and energy frameworks[14] (which we can expand as energy frameworks of the synthon modules[16]) allows visualization, interpretation and prediction of supramolecular reactions.

Experimental

All reactions and manipulations were performed using standard Schlenk techniques under an inert atmosphere of pure nitrogen or argon. Solvents were purified, dried and distilled under a nitrogen atmosphere prior to use. Commercial $[CymRuCl_2]_2$, KI, 4CNpy, and *o*-, *m*- and *p*-DITFBs were used without additional purification. $CymRuCl_2(4CNpy)$[26] and C_2I_2 (ref. 35) were prepared according to the reported procedures.

Preparation of $CymRuI_2(4CNpy)$

50 mg (~0.3 mmol) of powdered KI was stirred with an orange solution of 40 mg (~0.1 mmol) $CymRuCl_2(4CNpy)$ in 5 ml of HPLC grade acetone for 6 h at ambient temperature. The resulting dark-orange reaction mixture was dried under vacuum and extracted with CH_2Cl_2 (3 × 5 ml). The extract was mixed with heptane (5 ml), concentrated to the half of the initial volume and kept at ~10 °C for 12 h. A red crystalline precipitate was separated, washed with hexane, dried in a vacuum and used for single crystal XRD investigation. Further concentration and cooling of the mother-liquor allowed the increase in the quantity of $CymRuI_2(4CNpy)$. Yield (50 mg) 84%. Calc. for $C_{16}H_{18}I_2N_2Ru$ (%): C 32.33; H 3.05; N 4.72. Found: C 33.52, H 2.61, N 5.15.

4CNpy-DIOFBu (1). Dissolving 10 mg (0.1 mmol) of 4CNpy and 25 μl (0.14 mmol) of DIOFBu in DCM (0.2 ml) and subsequent slow evaporation of the solvent at room temperature for 48 h afforded XRD quality colorless crystals.

4CNpy-C_2I_2 (2). A clear colorless solution of 4 mg (0.025 mmol) of 4CNpy and 10 mg (0.036 mmol) of C_2I_2 in heptane (0.2 ml) was kept at ~10 C for 48 h. The mother liquor was decanted from the colorless crystalline precipitate. Long crystals of XRD quality were immediately used for single crystal XRD analysis. After being placed on a microscope glass, crystals show visible signs of decomposition within a few hours.

4CNpy – *p*-DITFB (3). Dissolving 10 mg (0.1 mmol) of 4CNpy and 40 mg (0.1 mmol) of *p*-DITFB in DCM (0.2 ml) and subsequent slow evaporation of the solvent at room temperature for 48 h afforded XRD quality colorless crystals.

4CNpy – *m*-DITFB (4). Dissolving 10 mg (0.1 mmol) of 4CNpy and 20 μL (~0.12 mmol) of *m*-DITFB in DCM (0.2 ml) and subsequent slow evaporation of the solvent at room temperature afforded an oily material which started to crystallize after 5 months and resulted in XRD quality colorless crystals.

[$CymRuCl_2$(4CNpy)]·DITFB (5). Dissolving 10 mg (0.025 mmol) of [$CymRuCl_2$(4CNpy)]·and 10 mg (0.025 mmol) of DITFB in DCM (0.2 ml) and subsequent slow evaporation of the solvent at room temperature for 48 h afforded XRD quality orange crystals.

[$CymRuI_2$(4CNpy)]·DITFB (6). Dissolving 15 mg (0.025 mmol) of [$CymRuI_2$(4CNpy)] and 10 mg (0.025 mmol) of DITFB in DCM (0.2 ml) and subsequent slow evaporation of the solvent at room temperature for 48 h afforded XRD quality red crystals.

Computational details

Intermolecular interaction energy calculation and subsequent energy framework generation for 4CNpy were performed using Crystal Explorer 17.5 (TONTO 18.10.24, B3LYP-DGDZVP)[14] for all the unique molecular pairs in the first coordination sphere of a molecule (3.8 Å), using experimental crystal geometries. For co-crystals **1–6**, the above procedure has been performed twice – separately for each unique co-former molecule in the asymmetric unit.[14,36]

MEP calculations were carried out with the ORCA 4.11 program package.[37] A non-hybrid PBE functional,[38] dispersion correction with Becke–Johnson damping (D3BJ)[39] and the def2-SVP basis set[40] with small-core pseudopotential for Te and I atoms[41] were used for geometry optimization. The def2/J auxiliary basis set[42] was used for Coulomb fitting. Electron density calculations on resulted geometries were performed using ZORA approximation for scalar relativistic effects,[43] and a hybrid functional PBE0 (ref. 44) and all-electron def2-TZVP[40] basis set was used for ZORA. RIJCOSX approximation[45] in combination with the SARC/J auxiliary basis set[46] was used to improve the computational speed. MEP extrema on the 0.002 e A^{-3} electron density isosurface were located using the Multiwfn program.[47]

Crystal structure determination

Relevant crystallographic data of **1–6** and $CymRuI_2$(4CNpy) are given in the ESI.†

A Bruker APEX II CCD area detector diffractometer equipped with a graphite-monochromated Mo Kα radiation source (0.71070 Å) was used for the cell determination and intensity data collection. The structure was solved by direct methods and refined by full-matrix least squares against F^2 using SHELXL and Olex2 software.[48,49] Non-hydrogen atoms were refined with anisotropic thermal parameters. All the hydrogen atoms were geometrically fixed and refined using a riding model. Atomic coordinates and other structural parameters have been deposited in the Cambridge Crystallographic Data Centre (CCDC 1940710 (**1**), CCDC 1941548 (**2**), CCDC 1940713 (**3**), CCDC 1955091 (**4**), CCDC 1940712 (**5**), CCDC 1940714 (**6**) and CCDC 1940711 for $CymRuI_2$(4CNpy)).

Conflicts of interest

There are no conflicts to declare.

Acknowledgements

This work is supported by the Russian Scientific Foundation (grant no. 19-13-00338). XRD experiments were performed using the equipment of shared experimental facilities supported by Kurnakov Institute of General and Inorganic Chemistry RAS.

References

1 E. V. Alexandrov, A. V. Virovets, V. A. Blatov and E. V. Peresypkina, *Chem. Rev.*, 2015, **115**, 12286–12319.

2 (*a*) S. Ferlay, O. Félix, M. W. Hosseini, J.-M. Planeix and M. Kyritsakas, *Chem. Commun.*, 2002, 702–703; (*b*) S. Ferlay, R. Holakovsky, M. W. Hosseini, J.-M. Planeix and N. Kyritsakas, *Chem. Commun.*, 2003, 1224–1225; (*c*) S. Ferlay, F. Bulach, O. Félix, M. W. Hosseini, J.-M. Planeix and N. Kyritsakas, *CrystEngComm*, 2002, **4**, 447; (*d*) P. C. Crawford, A. L. Gillon, J. Green, A. G. Orpen, T. J. Podesta and S. V. Pritchard, *CrystEngComm*, 2004, **6**, 419.

3 (*a*) M. Fourmigué and P. Batail, *Chem. Rev.*, 2004, **104**, 5379; (*b*) T. Imakubo, H. Sawa and R. Kato, *J. Chem. Soc., Chem. Commun.*, 1995, 1667; (*c*) H. M. Yamamoto, Y. Kosaka, R. Maeda, J. Yamaura, A. Nakao, T. Nakamura and R. Kato, *ACS Nano*, 2008, **2**, 143; (*d*) T. Imakubo, N. Tajima, M. Tamura, R. Kato, Y. Nishio and K. Kajita, *J. Mater. Chem.*, 2002, **12**, 159; (*e*) K. Ueda, T. Sugimoto, C. Faulmann and P. Cassoux, *Eur. J. Inorg. Chem.*, 2003, **12**, 2333; (*f*) L. Ouahab, F. Setifi, S. Golhen, T. Imakubo, R. Lescouëzec, F. Lloret, M. Julve and R. Świetlik, *C. R. Chim.*, 2005, **8**, 1286; (*g*) T. Imakubo, T. Shirahata, M. Kibune and H. Yoshino, *Eur. J. Inorg. Chem.*, 2007, **30**, 4727.

4 T. Imakubo, H. Sawa and R. Kato, *Synth. Met.*, 1995, **73**, 117–122.

5 R. Bertani, P. Sgarbossa, A. Venzo, F. Lelj, M. Amati, G. Resnati, T. Pilati, P. Metrangolo and G. Terraneo, *Coord. Chem. Rev.*, 2010, **254**, 677–695.

6 A.-L. Barrès, A. El-Ghayoury, L. V. Zorina, E. Canadell, P. Auban-Senzier and P. Batail, *Chem. Commun.*, 2008, 2194–2196.

7 J. E. Ormond-Prout, P. Smart and L. Brammer, *Cryst. Growth Des.*, 2012, **12**, 205–216.
8 L. Brammer, G. M. I. Espallargas and S. Libri, *CrystEngComm*, 2008, **10**, 1712–1727.
9 (*a*) G. R. Desiraju, *Chem. Commun.*, 1997, 1475–1482; (*b*) D. S. Reddy, B. S. Goud, K. Panneerselvam and G. R. Desiraju, *J. Chem. Soc., Chem. Commun.*, 1993, 663–664; (*c*) R. E. Meléndez and A. D. Hamilton, Hydrogen-Bonded Ribbons, Tapes and Sheets as Motifs for Crystal Engineering, *Design of Organic Solids*, 1998, pp. 97–129.
10 G. Lopes, V. da Gama, D. Belo, D. Simão, I. Cordeiro Santos, M. Almeida and S. Rabaça, *CrystEngComm*, 2019, **21**, 637–647.
11 C. R. Groom, I. J. Bruno, M. P. Lightfoot and S. C. Ward, *Acta Crystallogr., Sect. B: Struct. Sci., Cryst. Eng. Mater.*, 2016, **72**, 171–179.
12 P. M. J. Szell, S. A. Gabriel, E. Caron-Poulin, O. Jeannin, M. Fourmigué and D. L. Bryce, *Cryst. Growth Des.*, 2018, **10**, 6227–6238.
13 C. B. Aakeröy, C. L. Spartz, S. Dembowski, S. Dwyre and J. Desper, *IUCrJ*, 2015, **2**, 498–510.
14 M. J. Turner, S. P. Thomas, M. W. Shi, D. Jayatilaka and M. A. Spackman, *Chem. Commun.*, 2015, **51**, 3691–3928.
15 P. Ganguly and G. R. Desiraju, *CrystEngComm*, 2010, **12**, 817–833.
16 Y. V. Torubaev, D. K. Rai, I. V. Skabitsky, S. Pakhira and A. Dmitrienko, *New J. Chem.*, 2019, **43**, 7941–7949.
17 A. Mukherjee, *Cryst. Growth Des.*, 2015, **15**, 3076–3085.
18 I. Nicolas, O. Jeannin, D. Pichon and M. Fourmigue, *CrystEngComm*, 2016, **18**, 9325.
19 W.-N. Zheng, *Acta Crystallogr., Sect. E: Struct. Rep. Online*, 2012, **68**, o1625.
20 C. B. Aakeröy, T. K. Wijethunga, J. Desper and C. Moore, *J. Chem. Crystallogr.*, 2015, **45**, 267–276.
21 C. B. Aakeröy, M. Baldrighi, J. Desper, P. Metrangolo and G. Resnati, *Chem. – Eur. J.*, 2013, **19**, 16240–16247.
22 Y. V. Torubaev, K. A. Lyssenko, P. Y. Barzilovich, G. A. Saratov, M. M. Shaikh, A. Singh and P. Mathur, *CrystEngComm*, 2017, **19**, 5114–5121.
23 C. Perkins, S. Libri, H. Adams and L. Brammer, *CrystEngComm*, 2012, **14**, 3033–3038.
24 E. Bosch, S. J. Kruse, H. R. Krueger and R. H. Groeneman, *Cryst. Growth Des.*, 2019, **19**, 3092–3096.
25 G. Campillo-Alvarado, C. Li, D. C. Swenson and L. R. MacGillivray, *Cryst. Growth Des.*, 2019, **19**, 2511–2518.
26 D. K. Gupta, A. N. Sahay, D. S. Pandey, N. K. Jha, P. Sharma, G. Espinosa, A. Cabrera, M. C. Puerta and P. Valerga, *J. Organomet. Chem.*, 1998, **568**, 13.
27 M. Borovina, I. Kodrin and M. Đaković, *Cryst. Growth Des.*, 2019, **19**, 1985–1995.
28 Y. Wang, W. Wu, Y. Liu and Y. Lu, *Chem. Phys. Lett.*, 2013, **578**, 38–42.
29 B. N. Ghosh, M. Lahtinen, E. Kalenius, P. Mal and K. Rissanen, *Cryst. Growth Des.*, 2016, **16**, 2527.
30 G. R. Desiraju and R. Parthasarathy, *J. Am. Chem. Soc.*, 1989, **111**, 8725–8726.
31 Y. V. Torubaev, I. V. Skabitskiy, P. Rusina, A. A. Pasynskii, D. K. Rai and A. Singh, *CrystEngComm*, 2018, **20**, 2258–2266.
32 K. Lisac and D. Cincic, *CrystEngComm*, 2018, **20**, 5955–5963.
33 X. Ding, M. Tuikka, K. Rissanen and M. Haukka, *Crystals*, 2019, **9**, 319.
34 S. Y. Oh, C. W. Nickels, F. Garcia, W. Jones and T. Friscic, *CrystEngComm*, 2012, **14**, 6110.
35 A. Webb, J. E. Klijn, P. A. Hill, J. L. Bennett and N. S. Goroff, *J. Org. Chem.*, 2004, **69**, 660–664.
36 http://130.95.176.70/wiki/index.php?title=Intermolecular_Interaction_Energies.
37 F. Neese, Software update: the ORCA program system, version 4.0, *WIREs Comput. Mol. Sci.*, 2017, e1327, DOI: 10.1002/wcms.1327.
38 (*a*) J. P. Perdew, K. Burke and M. Ernzerhof, *Phys. Rev. Lett.*, 1996, **77**, 3865; (*b*) J. P. Perdew, K. Burke and M. Ernzerhof, *Phys. Rev. Lett.*, 1997, **78**, 1396 (Erratum).
39 (*a*) S. Grimme, S. Ehrlich and L. Goerigk, *J. Comput. Chem.*, 2011, **32**, 1456; (*b*) S. Grimme, J. Antony, S. Ehrlich and H. Krieg, *J. Chem. Phys.*, 2010, **132**, 154104.
40 F. Weigend and R. Ahlrichs, *Phys. Chem. Chem. Phys.*, 2005, **7**, 3297.
41 K. A. Peterson, D. Figgen, E. Goll, H. Stoll and M. Dolg, *J. Chem. Phys.*, 2003, **119**, 11113–11123.
42 F. Weigend, *Phys. Chem. Chem. Phys.*, 2006, **8**, 1057.
43 (*a*) E. van Lenthe, E. J. Baerendsand and J. B. Snijders, *J. Chem. Phys.*, 1993, **99**, 4597; (*b*) C. van Wullen, *J. Chem. Phys.*, 1998, **109**, 392.
44 C. Adamo and V. Barone, *J. Chem. Phys.*, 1999, **110**, 6158–6170.
45 R. Izsák and F. Neese, *J. Chem. Phys.*, 2011, **135**, 144105.
46 D. A. Pantazis and F. Neese, *Theor. Chem. Acc.*, 2012, **131**, 1292.
47 T. Lu and F. Chen, *J. Comput. Chem.*, 2012, **33**, 580–592.
48 G. M. Sheldrick, *Acta Crystallogr., Sect. C: Struct. Chem.*, 2015, **71**, 3–8.
49 O. V. Dolomanov, L. J. Bourhis, R. J. Gildea, J. A. K. Howard and H. Puschmann, *J. Appl. Crystallogr.*, 2009, **42**, 339–341.

